

DYNAMIC ABSORPTION INTO SIMULATED POROUS STRUCTURES

Cathy J. Ridgway and Patrick A. C. Gane

Omya AG
CH 4665 Oftringen
Switzerland

ABSTRACT

A computer model, Pore-Cor¹, has been used to simulate the permeation of fluid into porous structures by applying a wetting algorithm for fluids undergoing both inertial and viscous dynamical absorption. These structures comprise cubic pores connected by cylindrical throats on a three-dimensional 10x10x10 position matrix. Previously, Pore-Cor has been used to simulate the void structure of porous media by fitting as closely as possible the simulated mercury intrusion curve of the model structure to that of the experimentally determined mercury intrusion curve of the actual sample. This refined model structure was then used to simulate the absorption of a number of different fluids and confirmation with experimental absorption data, adopting the same fluid, provided the necessary confidence in the model. Based on this practical experience, the framework is developed from experimental comparison so that Pore-Cor can now be applied as a 'predictor' tool rather than a simulator of existing experimental results. The structures used here have been generated with the aim of isolating certain parameters so their influence on the absorption behaviour of a fluid can be identified. It is shown how, keeping the porosity constant, structures can be represented in a number of different ways and that these structures will have vastly different absorption behaviour. Reducing the value of the fluid density in the simulation has also been investigated to show where the transition occurs in the absorption behaviour from the linear t -dependent short timescale inertial Bosanquet regime to the \sqrt{t} Lucas-Washburn viscous regime. Such a system of connecting pores is representative of pigmented paper coating structures and, for example, by changing the particle size distribution of the pigment under suitably modified calendaring conditions, pore structures of equal porosity could exist in practice and have drastically different effects on fluid absorption. Implications on, say, the way an ink would set on the coating surface, can have dramatic practical significance. To be able to predict these effects and to design optimal coating structures for the fluids and inks used in a variety of printing, lacquering and glueing processes is seen as a significant advance, obviating the need for expensive matrix-designed production trialling.

Keywords: porous media, absorption, printing, ink setting, fluid-solid interactions, modelling.

¹ Pore-Cor is a software program of the Environmental and Fluids Modelling Group, University of Plymouth, PL4 8AA U.K.

INTRODUCTION

Absorption-controlled mechanisms dominate the field of papermaking and printing as well as being of relevance in a wide variety of other industrial and natural applications. Predicting the absorption behaviour of a given fluid in contact with the surface of a defined porous medium has for long been the target of research into computer modelling of simulated structures. The progress in such modelling has been based initially on the development of simulated structures which mimic the intrusion properties of real experimental samples. Mercury intrusion, for example, is a well established method for describing the pore size distribution, though it might be better defined as the resistance distribution to a non-wetting fluid. Together with the correction terms provided in conventional mercury compression and the more recently established techniques for accounting for compressible skeletal structures, such as the latex component in paper coatings (1), defined by the software Pore-Comp², the method allows these data to form the basis for establishing an equivalent simulated structure.

However, two further steps were needed to translate a useful representation of a structure into a valuable predictive tool. This was achieved by the work of the authors and other co-workers (2-5) in which the identification of a suitable dynamic algorithm was combined with the necessary geometrical realism to establish a simulation for absorption of a wetting fluid. The complexities of absorption, particularly at the short timescales prevalent in many of the processes associated with coated paper and board printing, finishing and converting, have to be accounted for. The biggest hurdle in achieving this aim was the clear experimental contradiction of the accepted viscous-controlled Lucas-Washburn absorption dynamic. It is well known that a gloss paper made of fine pigments distributed in the coating structure, with often a relatively low porosity, imparts a rapid absorption dynamic and is manifest as a very rapid ink tack and setting characteristic. On the other hand, a matt paper coating of high porosity imparts a slow ink setting despite the larger pore size involved. This is one example where a simple capillary model, based on Lucas-Washburn, fails on the basis of a linear capillary radius dependence of the absorption rate. Furthermore, paper coating designers increasingly desire the decoupling of absorption rate from the overall porosity of the sample (6) to allow for the absorption of multiple fluid components which exist over discretely differing viscosity and volume ranges; for example low viscosity mineral oil vehicles and high viscosity linseed oil resin-solving components in inks, which, together with water-based fountain solution, constitute the offset printing process as experienced by the paper surface (7, 8). Modified particle size distributions (6, 9-11) and costructured pigments incorporating distinctly different surface chemistries (12) are some of the ways being trialled to achieve differential absorption characteristics.

An algorithm incorporating short timescale inertial retardation, which affects a slowing of entry into the larger pores and initiates a short-lived linear time dependence in the finer pores, together with the longer term viscous drag component typified in the Lucas-Washburn relation, was achieved using a solution of the Bosanquet equation (13) in which momentum considerations, avoiding the

² Pore-Comp is a software program of the Environmental and Fluids Modelling Group, University of Plymouth, PL4 8AA U.K.

discontinuity of initial $t = 0$ acceleration by averaging techniques, form the basis for a time decaying function of the second of Newton's laws of motion applying to the inertia of a column of fluid mass entering a pore. For, say, water and thin mineral oils, (4), this occurs within the first $\leq 0.1 \mu\text{m}$ in a time scale of $\sim 10 \text{ ns}$. Denser low viscosity fluids have a longer lasting inertial effect. More viscous fluids have a shorter-lived inertial effect. The match to experimental absorption data into predetermined bulk structures was achieved and further developed using conically modified geometries of the connecting throats in the model (4). This basis of agreement forms the confidence level needed to move forward to using the Pore-Cor and associated Bosanquet wetting algorithm as a predictor of absorption dynamic.

Presented below are some of the effects that can be simulated using these techniques including the vexing question of what pore size distribution provides for the necessary short time and long time porosity characteristics needed to achieve optimal print performance. The data illustrate the discontinuous dynamic as the porosity and pore size distribution are modelled as independent variables to form a contour behaviour from which the design criteria can ultimately be determined.

THE PORE-COR¹ NETWORK MODEL

The unit cell

Pore-Cor is a computer model that simulates the void-space structure of porous materials. It has been used to simulate the structures of a wide range of porous materials including sandstones (14), medicinal tablets (15) and soil (16). Pore-Cor uses a unit cell with 1 000 cubic pores in a three dimensional $10 \times 10 \times 10$ array, connected by up to 3 000 throats, which in this work are assumed cylindrical, (i.e. one connected to each cube face). Each pore is equally spaced from its neighbouring pores by the 'pore row spacing' Q , and each unit cell is a cube of side length $10 Q$. There are periodic boundary conditions, which are applied serially during wetting, with each cell connected to another identical unit cell in each direction. When used to simulate actual samples the pore- and throat-size distributions of the unit cell are optimised so that the simulated percolation curve fits as closely as possible to the experimental mercury intrusion curve (17), corrected for mercury compression, penetrometer expansion and sample compression (1). The distribution of throat sizes is log-linear and the actual number of each pore and throat size is characterised by the parameter 'throat skew'. The throat skew is the percentage number of throats of the smallest size and the linear distribution pivots about its mid-point at 1%. The positions of the pores and throats are random, determined by a pseudo-random number generator. The throats are randomly positioned within the array and the pores are then generated to be the size of the largest throat entering them.

A matrix of values of throat skew and connectivity (the average number of throats per pore over the whole unit cell) are refined on a trial basis, and the void structure which has percolation characteristics most closely matching the experimental values (17) is selected (16). The percolation characteristics of the network are insensitive to Q . Therefore, the Q value of the chosen structure is adjusted so that its porosity matches the experimental value while ensuring that no pores overlap. It is not normally possible to represent the full true complexity of the void network of a natural sample

using the relatively simple geometry of the Pore-Cor unit cell. One reason is that the size of the unit cell is often smaller than the representative elementary volume (REV) of the sample. Therefore, different unit cells must be generated using different seeds for the pseudo-random number generator. The algorithm is designed so that different structural parameters in conjunction with the same seed of the pseudo-random number generator produce a family of unit cells which are similar to each other; for example, all may have a group of large pores in the same region (16). Different stochastic generations use a different pseudo random number generator seed, and can either use the original Pore-Cor optimisation parameters or can be re-optimised to the experimental data.

In the case of paper and board coatings, however, the limitation of the unit cell size is usually manifest only in the xy plane parallel to the paper surface, whilst the dimension of the z direction of the unit cell is often sufficient. If continuity is considered in the xy plane of applied thin films of fluid, or even droplets, the continuity of supersource conditions can be applied easily in relation to the xy dimensions of the unit cell and the uniaxial $-z$ direction absorption is well represented.

The wetting algorithm

The work of the authors and co-workers (3, 5) establishes the necessary theoretical background for the absorption model. This begins with a description of the solution of the wetting algorithm into an idealised capillary and is then extended to the case of the interconnected pore structure model.

(i) absorption into an idealised capillary

The simplest case for the description of capillarity is represented by a horizontal circular tube of definably small radius, r_c . The Laplace pressure, P , across the meniscus of a fluid being absorbed describes the force of imbibition of the capillary and is given by the curvature of the liquid/gas (air) meniscus.

$$P = \frac{2g_{LV} \cos q}{r_c} \quad (1)$$

The contributing factors are the contact angle, q , which is the result of the 3 phase interaction consisting mainly of the cohesive forces of the liquid (surface tension g_{LV} , more precisely the liquid-vapour interfacial tension) which tend to form a surface of minimal energy, which for a free liquid surface would be spherical, and the adhesion forces of the solid-liquid interface attracting the liquid in an attempt to cover the solid and so reduce the apparent free surface energy. If complete wetting occurs, q is zero and the solid-liquid tension, g_{SL} , is at a maximum. Any deviation of q from zero lowers the wettability and therefore the intrinsic wetting force of the liquid front. The other important component of equation (1) is the radius, r_c , of the capillary. It is easy to see that the smaller the radius the greater the driving pressure or capillary force. This driving force would be a perpetual mobile if there were no frictional and turbulent dissipation of energy.

To obtain an equation of dynamic motion, the Laplace relation is traditionally incorporated into Poiseuille's equation of laminar flow for a liquid of viscosity \mathbf{h} : this was introduced by Lucas (18) and Washburn (19) and they obtained the well-known relation of:

$$x^2 = \left(\frac{r_c t}{2\mathbf{h}} \right) \mathbf{g}_{LV} \cos \mathbf{q} \quad (2)$$

where x is the distance travelled by the liquid front after time, t , in an hypothetical horizontal tube.

This equation (2), however, has some major drawbacks. The main drawback is the lack of inertial terms, relating to the mass of fluid under motion, as was recognised by Rideal (20). The practical relevance of inertia in capillary uptake was elegantly shown by Quéré using a high speed camera to detect the meniscus position in a small tube (21).

Bosanquet (13) complemented Rideal's solution in 1923 adding the inertial impulse drag effect associated with an accelerating fluid of density \mathbf{r} , giving the following force balance:

$$\frac{d}{dt} \left(\mathbf{p} r_c^2 \mathbf{r} x \frac{dx}{dt} \right) + 8\mathbf{p}\mathbf{h}x \frac{dx}{dt} = P_e \mathbf{p} r_c^2 + 2\mathbf{p} r_c \mathbf{g}_{LV} \cos \mathbf{q} \quad (3)$$

where P_e is the external pressure, if applied, at the entrance of the capillary tube, equation (1).

By integration, and letting

$$a = \frac{8\mathbf{h}}{\mathbf{r} r_c^2} \quad b = \frac{P_e r_c + 2\mathbf{g}_{LV} \cos \mathbf{q}}{\mathbf{r} r_c} \quad (4)$$

it can be shown that

$$x_2^2 - x_1^2 = \frac{2b}{a} \left\{ t - \frac{1}{a} (1 - e^{-at}) \right\} \quad (5)$$

where x_1 is the initial position and x_2 is the position after time t .

Taking equation (5), where for $at \ll 1$, i.e. short timescales, and using a Taylor series expansion,

$$e^{-at} = 1 - at + \frac{a^2 t^2}{2} \quad (at \ll 1) \quad (6)$$

From equation (5), it then follows that,

$$x_2^2 - x_1^2 = bt^2 \quad (at \ll 1) \quad (7)$$

If the measurement coordinates are set such that x_1 is zero and there is no applied external pressure P_e , then

$$x^2 = \frac{2g_{LV} \cos \theta t^2}{r_c \rho} \quad (at \ll 1, P_e = 0) \quad (8)$$

This equation describes what is referred to as 'inertial flow'. The distance travelled, x , is directly proportional to time t , in contrast to the Laplace-Poiseuille flow regime described by the Lucas-Washburn equation (2) for which $x \propto \sqrt{t}$. Also, in contrast, the distance travelled by inertial flow is independent of viscosity, and inversely related to the radius of the tube, r_c , and the fluid density, ρ .

Under the conditions of inertial uptake, the regime of equation (8) describes a monolithic block of fluid entering a tube, driven by the wetting force of the liquid contacting the initial sidewalls of the tube. The fluid is assumed to have a flat meniscus front, except in practice at the actual wall contact, and all parts of the fluid within the tube move at the same rate: hence the initial independence from viscosity. The flow is retarded more for a high density fluid entering a large tube because the mass of fluid, and hence its inertia, is higher. Also, the higher the viscosity of the fluid, the sooner the effect of viscous drag becomes apparent.

The effect of inertial retardation and subsequent introduction of viscous drag is shown quantitatively in Fig. 1 for propandiol (viscosity 57.1 mPas) entering capillaries of contrasting radii of 1 μm and 1mm, respectively.

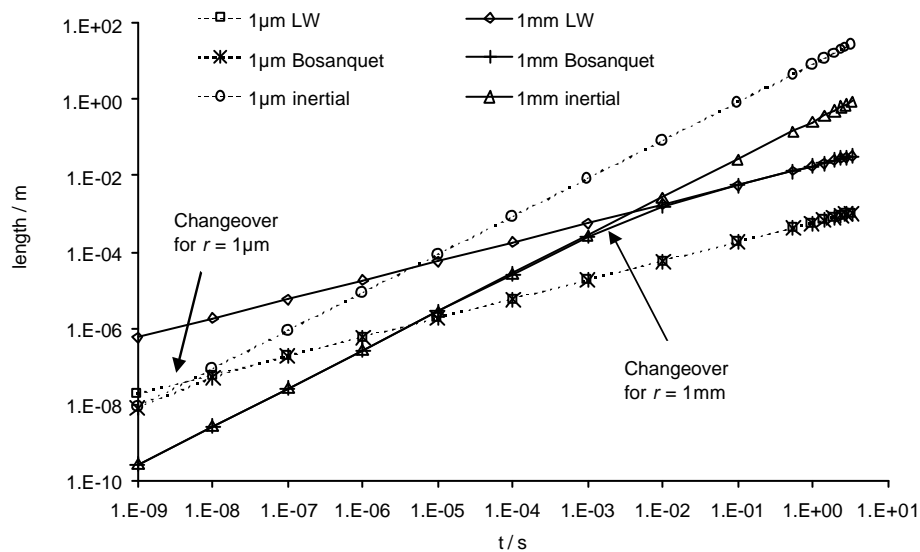


Fig. 1 Comparison of inertial and viscous equations and Bosanquet's solution for propandiol (taken from Schoelkopf *et al.* (3)).

The graphs show how the proposed (Bosanquet) flow changes from inertial to Lucas-Washburn (LW) flow as time and distance increase. For a tube of 1 mm radius, the change-over begins at about 0.01 s and after 1 mm penetration, and for a tube of radius 1 μm it starts at about 0.01 μs and 0.1 μm absorption distance. For even smaller tubes, the change-over will occur even faster and earlier, so that the flow will be accurately described by the Lucas-Washburn solution more quickly in the finest of capillaries for supersource conditions. With increasing fluid viscosity, whilst keeping fluid density and tube radius constant, the change-over will occur earlier which shows that viscosity and radius are in a mutual relationship through frictional dissipation compared with the density and radius in turn determining inertia.

(ii) absorption into the interconnecting pore structure

The Bosanquet equation (13) is now used to calculate the wetting flux in each pore and throat in the void network at every time step. It is assumed that inertial flow occurs when fluid begins to enter each throat, initially wetting the throat in the form of a monolithic block of fluid as described previously (3, 5). Once a throat is full, the volumetric flow rate of the fluid leaving the throat is calculated and this fluid starts to fill the connected pore. The pore can be filled by fluid from more than one throat, which may start to flow into it at different times. Once a pore is full, it starts to fill the throats connected to it that are not already full and which are not already filling from other pores. If at any stage the outflow of a pore exceeds the inflow then a mass conservation restriction is applied which removes this imbalance and restricts the further fluid flow into the network.

At the start of the calculation for wetting into the simulated Pore-Cor structure, the total time length for the absorption is specified. The maximum length of a time step is 1 ns (nanosecond), its value being such that the maximum distance advanced by the fluid in one time step is never more than $0.1 Q$. There is also a further restriction on the length of the time step in order to prevent an oscillatory flow behaviour in the throats with the smaller radii as explained by Ridgway *et al.* (4). This occurs if $r^2 \mathbf{r} / 4\mathbf{h}$ is less than 1ns, where r is the minimum throat radius in the structure. In this case the time step is set to $r^2 \mathbf{r} / 4\mathbf{h}$. The flow rate varies greatly with throat diameter, with the consequence that many millions of timesteps must be calculated. The absorption is quantified as F , the fraction of the total void volume in the unit cell which is filled with the fluid at time t .

PARAMETRISING THE SYNTHESISED STRUCTURES

Pore-Cor is used here to simulate a range of predefined structures in order to investigate the effects on the absorption of a fluid both in respect to the composition of the void space of the unit cell and in respect to the fluid density and viscosity relating these effects to known experience in respect to paper coatings. Recent modelling and experimental observations by Gane *et al.* (2) and Schoelkopf *et al.* (5) have highlighted the possibility of developing rapid absorption properties with respect to water and low viscosity oils by concentrating the pore size distribution of porous media within the 0.05 to 0.1 μm region. This leads to a concentration of the otherwise differentiating preferred pathway dynamic of absorption caused by inertial retardation of short timescale imbibition into larger pores. At short time the absorption is linear

with time t , acting through the shortest, finest capillaries before laminar Poiseuille viscous drag can be established over these short distances. In larger pores the fluid is momentarily retarded due to the mass which has to be accelerated according to Newton's Law, and the absorption proceeds subsequently by the familiar \sqrt{t} relationship of Lucas-Washburn. For this reason a pore size distribution concentrated around $0.1 \mu\text{m}$ has been chosen to represent the majority of these simulations lying around the expected pore-size transition point between inertial and viscous wetting for the fluids of interest.

Idealised monosized pore structures

a) Effect of throat length

Pore-Cor generates 100 different sized throats spread equally over a logarithmic axis between the minimum and maximum throat diameters. By entering into the model almost identical settings for the minimum and maximum diameters, in fact with a narrow distribution of $\pm 0.001 \mu\text{m}$ between the maximum and minimum, an effectively mono-sized distribution is obtained. A series of unit cells with $0.1 \mu\text{m}$ 'monosized' throats (and hence pores) was generated and the porosity was used as a control parameter to adjust the pore row spacings within the unit cell, Fig. 2. This figure demonstrates visually the structural effect of changing the throat length connecting the pores within a structure. The Pore-Cor parameters used to generate these structures are shown in Table 1. The pore and throat size distribution remains the same, i.e. the number of and diameter of the pores and throats remain the same, but the throat length is decreased as the desired porosity is increased. The connectivity of these structures is set at the maximum value of 6. The relevant absorption curves for these structures using the wetting algorithm described above are shown in Fig. 3.

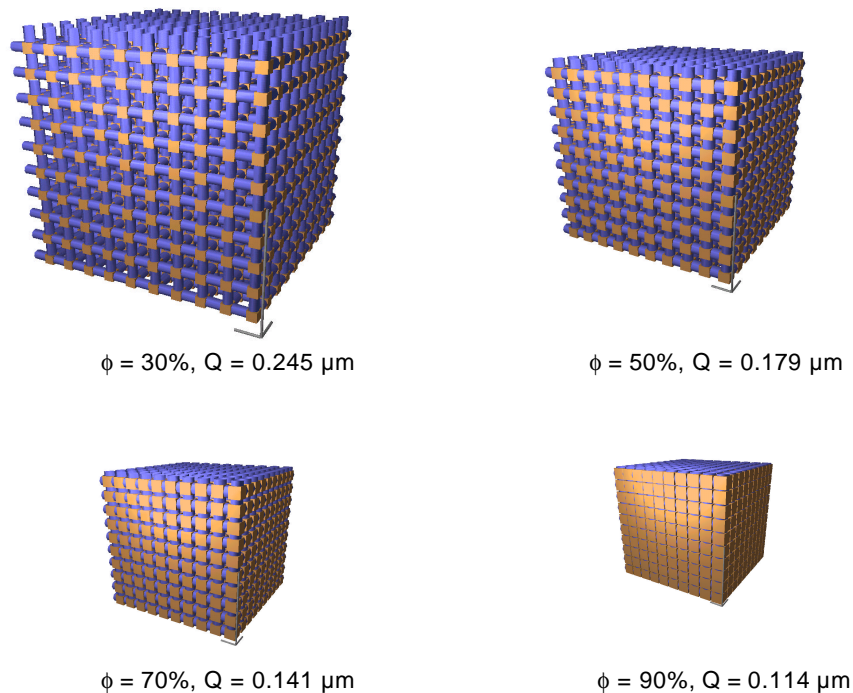


Fig. 2 Structures generated for a range of porosities using constant monosize pores (set to $0.1 \mu\text{m}$). These structures are used to study the effect of throat length.

Minimum diameter / μm	Maximum diameter / μm	Throat skew	Connectivity	Porosity, f / %	Pore row spacing, Q / μm
0.099	0.101	1	6	30	0.245
0.099	0.101	1	6	50	0.179
0.099	0.101	1	6	70	0.141
0.099	0.101	1	6	90	0.114

Table 1 Parameters used for the model structures in Fig. 1.

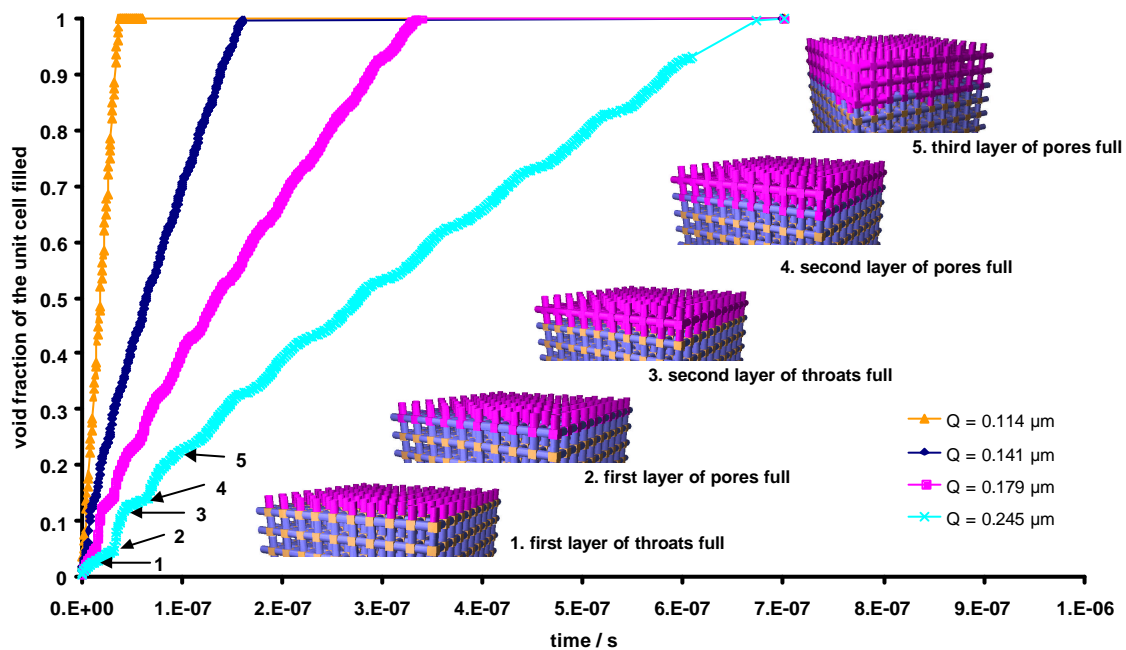


Fig. 3 Increasing pore row spacing with a monosize pore and throat diameter distribution of $0.1 \mu\text{m}$. Pore row spacing is modified through the adjustment of porosity as shown in Fig. 1, showing the effect of changing throat length.

The overall trend of the curves shown in Fig. 3, as the pore row spacing Q increases, shows that the longer the throats, the slower the absorption rate. The absorption moves from the linear t dependency regime of the Bosanquet equation to the \sqrt{t} dependency of Lucas-Washburn as viscous drag is established in the longer throats.

Changing porosity whilst keeping the basic pore size constant is a particular case where the effect of connecting geometry can be studied. As particles of pigment become more asymmetric, so the porous structure becomes more anisotropic. For example, as one moves from an isometric coating structure of blocky ground calcium carbonate, or fine glossing US clay, progressively toward a disordered anisometric coating of high aspect ratio platelets or needles, such as English clay, talc or aragonitic precipitated calcium carbonate, and then further toward ordered anisometric coatings of such high aspect ratio particles, so the connecting throats are effectively elongated often in a preferred direction. In these cases, it can be expected

that the imbibition rate of the coating will slow toward a more Lucas-Washburn type permeation rate. Traditionally this used to be expressed as an increase in so-called tortuosity, a convenient term used to describe the extension of the path length required to be followed by the fluid to occupy the same void volume. Here it can be seen that the actual dynamic changes from inertial to viscous drag as the "aspect ratio" between pores and throat length increases effectively providing an insight into the effects of tortuosity.

Close inspection of the absorption of water (surface energy, $\gamma_{LV} = 0.07275 \text{ Nm}^{-1}$, contact angle, $\theta = 0^\circ$, viscosity, $\eta = 0.001 \text{ kgm}^{-1}\text{s}^{-1}$ and density, $\rho = 998 \text{ kgm}^{-3}$) for the structure with $Q = 0.245 \text{ }\mu\text{m}$ shows that the curve is not smooth, but has regular bumps. These bumps are an artefact of this particular artificially regular structure within the unit cell and the stepwise way in which the algorithm calculates the flow rate through the unit cell in respect to the repeat boundary condition of its nearest neighbours. There is a smooth transition between the filling of the first layer of throats, position 1, and the first layer of pores, as the pores are designated to fill at the final flow rate exiting from the top layer of throats. The first bump occurs at $3.2 \times 10^{-8} \text{ s}$, shown as position 2 in Fig. 3. At this point, both the first layer of throats and the first layer of pores are full. Once a layer of pores is full, the subroutine sequentially steps through each pore and starts to fill any empty throats adjoining it. For this reason there is an artificial sideways 'sweep' across the unit cell as it fills. As all these throats fill there is a significant increase in the fractional void volume filled over a short period of time, position 3. These steps in the curve occur each time the next layer of pores are full and the adjoining throats, both lateral and in the next layer, start to fill, positions 4 and 5.

Although the step-wise filling jump seen after every throat-pore layer pair is an artefact of the system, and only applies to the particularly regular arrays used here, it actually mimics well the Gibbs hinging phenomenon described by Knackstedt, Senden and Lyne (22), in which it was shown by physical micro-modelling that as an imbibing fluid reaches a discontinuous boundary, such as would be found in an artificial regular array of connecting rectangular tubes, there is a delay which occurs over an as yet mathematically undefinable time during which the meniscus front hinges about the discontinuity before proceeding rapidly once a wetting configuration is re-established. Because the mathematics of the phenomenon is so intractable, the sequential boundary condition and 'sweep' sequencing intrinsic to the Pore-Cor wetting algorithm is in fact ideally suited to modelling this effect.

b) Changing connectivity

(i) keeping the pore row spacing constant - changing porosity

A series of unit cells were generated, again with a monosize pore and throat diameter distribution of $0.1 \text{ }\mu\text{m}$. The connectivity was reduced progressively from 6 to 3. By reducing the connectivity some throats are removed from the structure. Therefore, by keeping the pore row spacing constant the porosity is reduced. This series of structures is shown in Fig. 4, and the reducing number of throats can be seen clearly on the top surface of the unit cell. The reduction of throats is not restricted to the top

of the unit cell but is spread throughout. The Pore-Cor parameters used to generate these structures are given in Table 2 and the absorption curves are shown in Fig. 5.

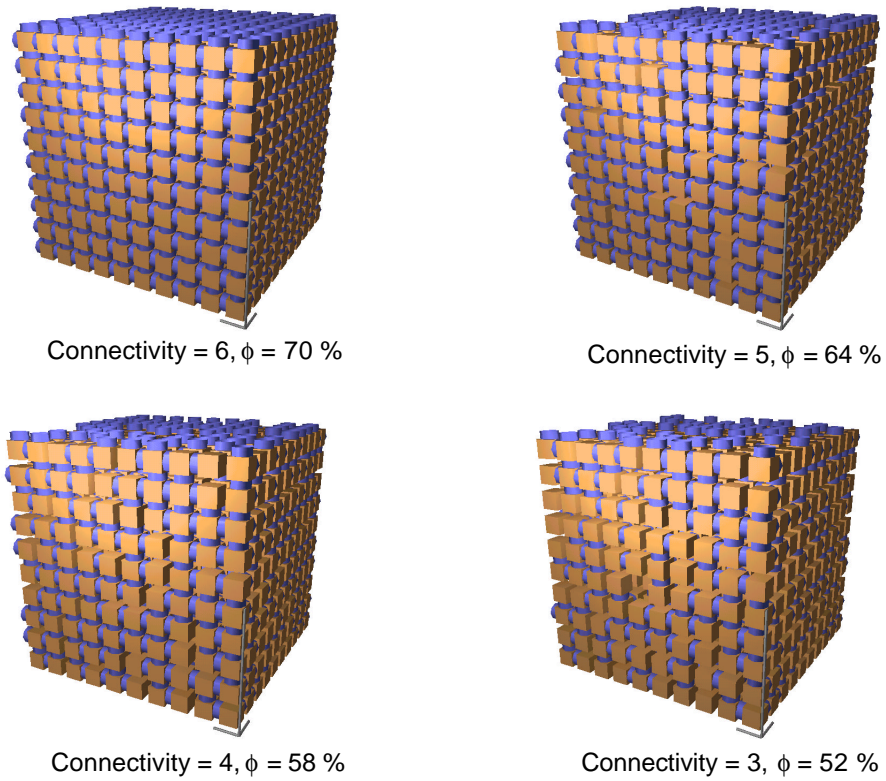


Fig. 4 Reducing connectivity, keeping the pore row spacing, Q , constant results in reduced porosity, f .

Minimum diameter / μm	Maximum diameter / μm	Throat skew	Connectivity	Porosity, f / %	Pore row spacing, Q / μm
0.099	0.101	1	6	70	0.141
0.099	0.101	1	5	64	0.141
0.099	0.101	1	4	58	0.141
0.099	0.101	1	3	52	0.141

Table 2 Pore-Cor parameters for the reduced connectivity structures shown in Fig. 4.

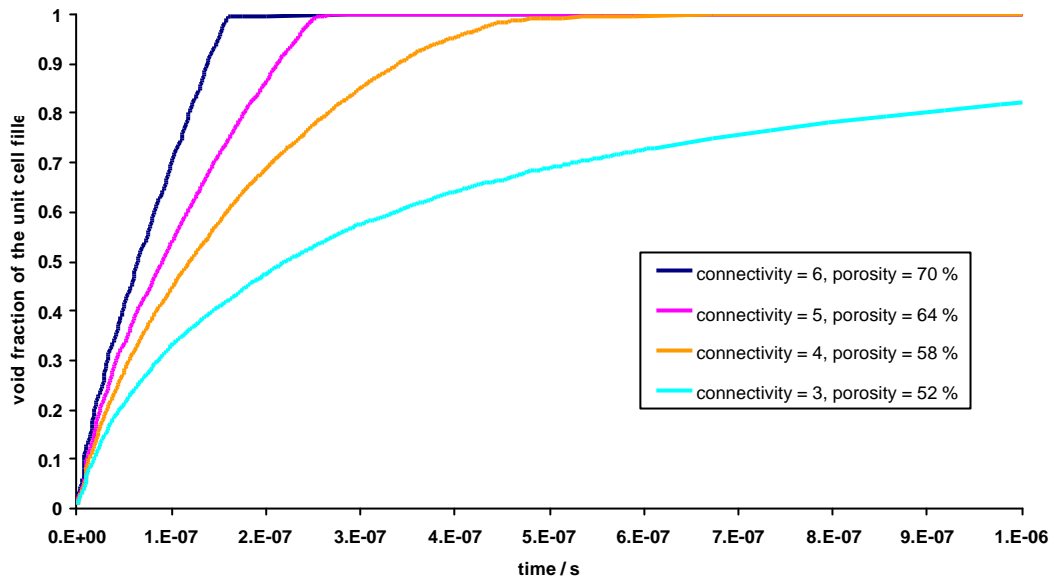


Fig. 5 Reducing connectivity whilst keeping pore row spacing constant for a monosize pore and throat diameter distribution (set to $0.1 \mu\text{m}$).

A structure with a connectivity of 6 results in the absorption being at its fastest rate. The steps in the curve are still just apparent due to the layering of pores and throats and the sideways spread restrictions in the algorithm. As the connectivity is reduced, the sideways increased rate step effect is removed as the regularity of the structure is disturbed. The pathways through the unit cell become less similar and more tortuous and therefore the path for filling is longer giving an overall reduced absorption rate. The mass balance will also cause the rate of filling to be reduced as some pores may have less fluid flowing into them since some throats are now removed. The outflow from the pores will also be further restricted.

The effect of reducing connectivity has an even greater effect than changing the throat length (compare Fig. 5 with Fig. 3). In paper coating the blocking effect of natural and synthetic binder films can be envisaged, which, in the defined case of non-interaction with the fluid, will lead to a progressive slowing of imbibition provided the binder does not reduce the effective pore size and is found to reside in the interconnecting structures only. This latter situation is similar to the case where minimal binder is used such as in rotogravure colours or heatset web offset grades. Once binder levels increase such that the pore size becomes affected then the picture becomes more complicated as will be shown later when the effect of pore size distribution is studied.

(ii) keeping porosity constant - changing pore row spacing

Structures are now studied in which the porosity is maintained while the connectivity changes. This effectively means that the pore row spacing in the model must change and the effect is then observed by the wetting algorithm. It is clear from Fig. 6 that the actual structures of these unit cells are visibly different for the same given porosity. The structure with the lower connectivity is more compact - it has the smallest value for Q . The Pore-Cor parameters are shown in Table 3, and the

absorption curves in Fig. 7 which show once again that for the structure with the lowest connectivity the absorption rate is the slowest.

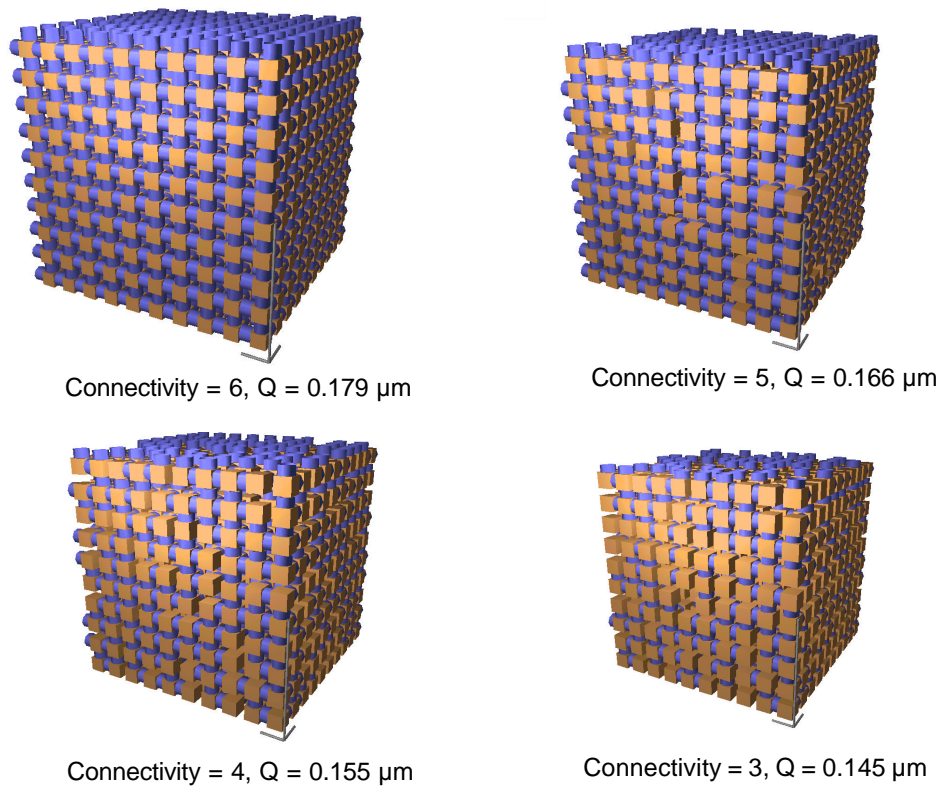


Fig. 6 Maintaining constant porosity whilst changing the pore structure in respect to connectivity and pore row spacing - the pore size is maintained constant.

Minimum diameter / μm	Maximum diameter / μm	Throat skew	Connectivity	Porosity, f / %	Pore row spacing, Q / μm
0.099	0.101	1	6	50	0.179
0.099	0.101	1	5	50	0.166
0.099	0.101	1	4	50	0.155
0.099	0.101	1	3	50	0.145

Table 3 Pore-Cor parameters for the structures shown in Fig. 6.

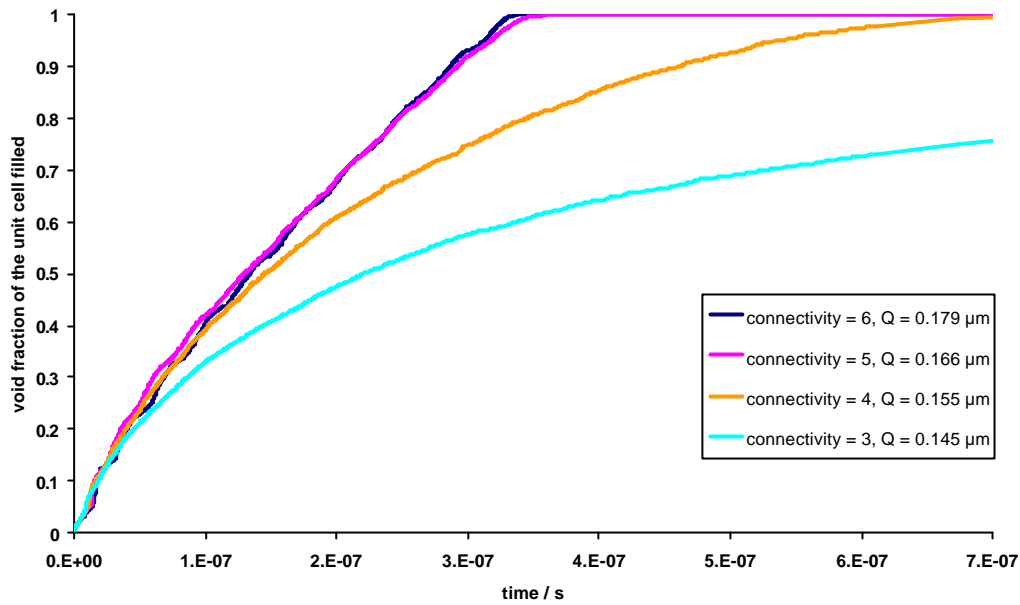


Fig. 7 Imbibition rates for the monosize pore structures shown in Fig. 6.

The rate of absorption follows the logical sequence in respect to decreasing connectivity. As connectivity decreases, so the pore row spacing decreases to maintain constant porosity, i.e. the decrease in throat length would enhance the absorption rate but this is masked by the effect of decreasing the connectivity. In the first decreasing step of connectivity (6 reducing to 5) the difference in throat length produces an apparently equal absorption enhancement which offsets the reduction in connectivity. However, as connectivity is reduced further the effect of the absorption-enhancing short throats becomes outweighed. The effect of keeping the porosity constant while changing connectivity, as seen by comparing Fig. 3 and Fig. 5 with Fig. 7, is to retard the absorption as the connectivity decreases. This effect is stronger than changing throat length alone, but not as strong as when the porosity decreases.

The retardational effect of reducing porosity, however, is a more evenly distributed function (Fig. 5), i.e. there is less "bunching" of the absorption curves at high porosity than is seen when throat length and connectivity are changed.

c) Effect of fluid parameters entering monosize pore structures of constant porosity

There are three factors contributing to the rate of absorption, (i) the inertial retardation term, which is independent of viscosity but directly dependent on the radius and the density, (ii) the short t timescale dependency regime, during which the fluid enters as an effective monolith, and in which the rate of absorption is inversely dependent on the entry throat radius, its duration being directly dependent on the density of the fluid but inversely on its viscosity and (iii) the longer \sqrt{t} regime, when the rate depends inversely on viscosity but directly on entry throat radius, and occurs sooner in narrow throats. The inertia initially slows down the rate of absorption, the t dependency will accelerate the absorption and the \sqrt{t} dependency again slows it down. By generating a series of unit cell structures and by following a progressive reduction of fluid density these effects are illustrated.

A series of differently sized ‘monosized’ distributions, ranging from 0.01 μm to 5 μm was generated. A connectivity value of 4 was used throughout, and a throat skew of 1 was adopted such that equal numbers of all possible throat sizes were used to develop a fixed porosity of 50 %. As a result, the pore row spacing, Q , scaled with the pore diameter increase, as shown in Table 4. A selection of these structures is shown in Fig. 8, and an illustration of equal areas of three different unit cells is shown in Fig. 9, illustrating the different structures sampled by equal areas of fluid contact.

Minimum diameter / μm	Maximum diameter / μm	Throat skew	Connectivity	Porosity, f / %	Pore row spacing, Q / μm
0.009	0.011	1	4	50	0.0154
0.019	0.021	1	4	50	0.0308
0.049	0.051	1	4	50	0.0769
0.099	0.101	1	4	50	0.1530
0.199	0.201	1	4	50	0.3070
0.499	0.501	1	4	50	0.7680
0.999	1.001	1	4	50	1.5300
1.999	2.001	1	4	50	3.0700
4.999	5.001	1	4	50	7.7400

Table 4 A variety of monosized pore structures, maintaining a constant porosity of 50 %

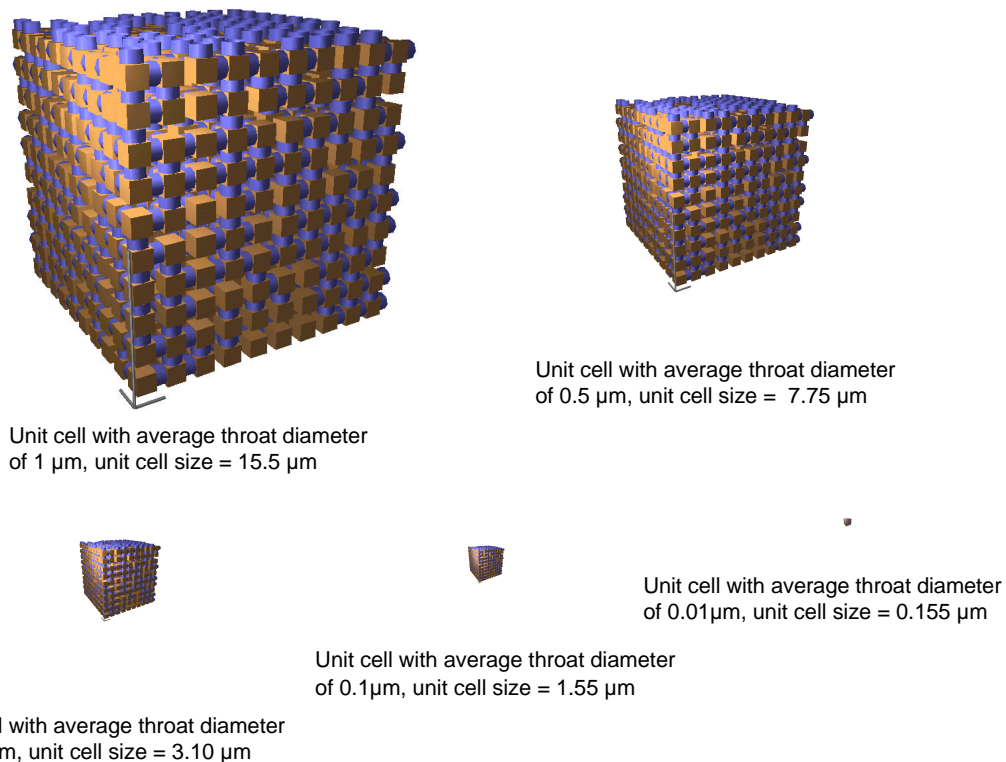


Fig. 8 Range of Pore-Cor unit cells of different *monosize* distributions, maintaining fixed porosity and connectivity (set to 50 % and 4, respectively).

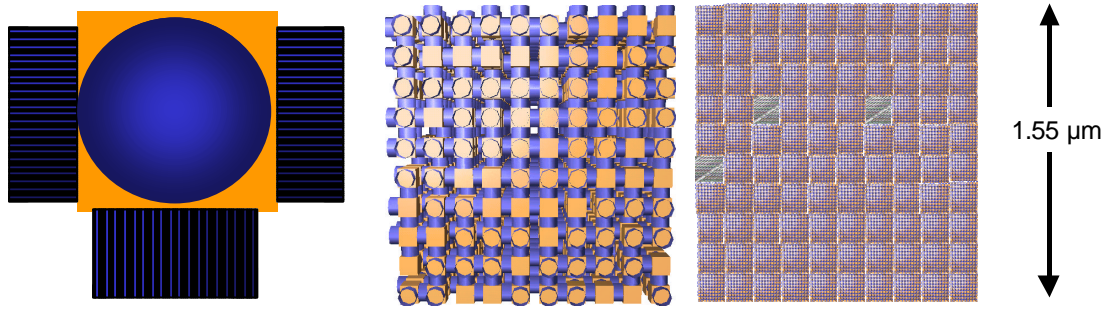


Fig 9. View of regions of equal area for unit cells of sizes 15.1 μm , 1.55 μm and 0.155 μm , respectively

(i) at fixed density and viscosity

The simulated absorption curves for water absorbing into these structures are shown in Fig. 10. The overall trend is that the smallest sized unit cell with the smallest pores and shortest throats absorbs at a much faster rate than the largest sized unit cell. Increasing pore size (the effective monosized pore and throat distributions) produces a trend of reducing absorption rate.

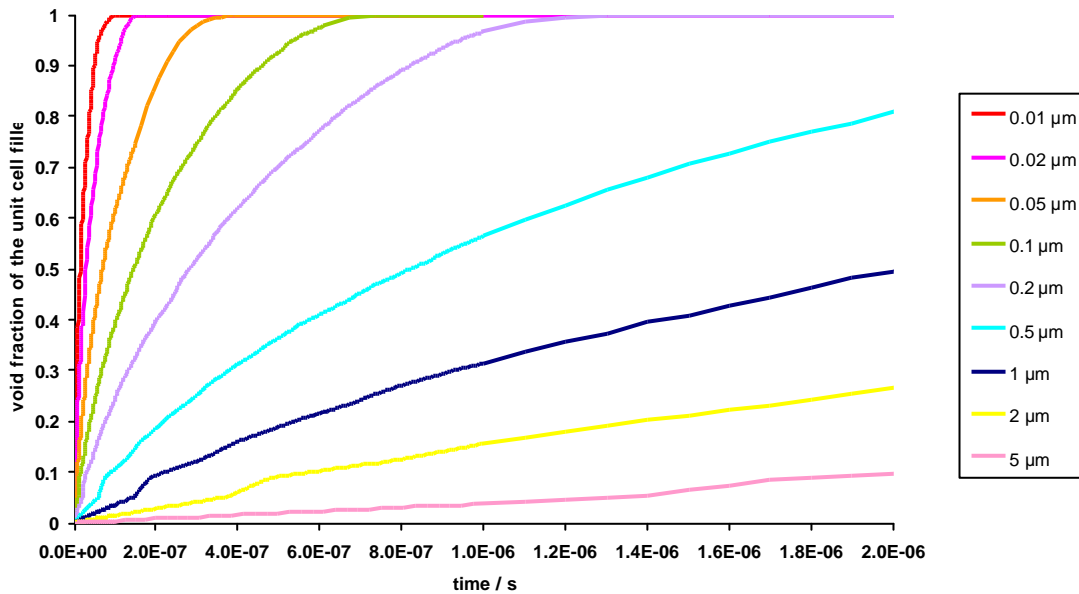


Fig. 10 Water absorption at fixed density and viscosity (998 kgm^{-3} and $0.001 \text{ kgm}^{-1}\text{s}^{-1}$) into the range of monosized pore sizes.

If the diameter of the throat is large then there is effectively no viscous drag but there is inertial retardation. If the length of the throat is short then the absorption time to fill the throat is short and absorption is t dependent as the viscosity will not have had time to have an influence on the rate, and there will be little viscous drag.

If the diameter of the throat is small enough, then the absorption is not inertially retarded but, depending on its length, the effect of viscosity will change. Short length

fine throats have t dependent filling, whereas longer fine throats quickly change to \sqrt{t} . However, pigments used in paper coatings usually have at least two similar axial dimensions, e.g. spheres have three and platelets have two, the exception is needle-like pigments. In such cases a large degree of similarity between pore size and length for blocky particles and extended throats for platelets can be assumed. Thus, for highly symmetrical systems like blocky particles, the simulation is quite suitable when the throat length is similar to the throat diameter, and in this case, the finest pores will continue to behave under linear t absorption until filled. For more complex geometries, the extended throat length will change the system over into \sqrt{t} .

The absorption curves in Fig. 10 are comparing different sized unit cells and so different volumes of fluid are also being compared. This may mask some effects and so to counteract this artefact the gradients from a plot of volume per unit cross-sectional area against time are compared to develop the physical relevance. These absorption rates are taken within the initial short time regime for each monosize pore unit cell. A three-dimensional plot is shown in Fig. 11 which shows the absorption rates over the range of monosized pore unit cells described in Table 4.

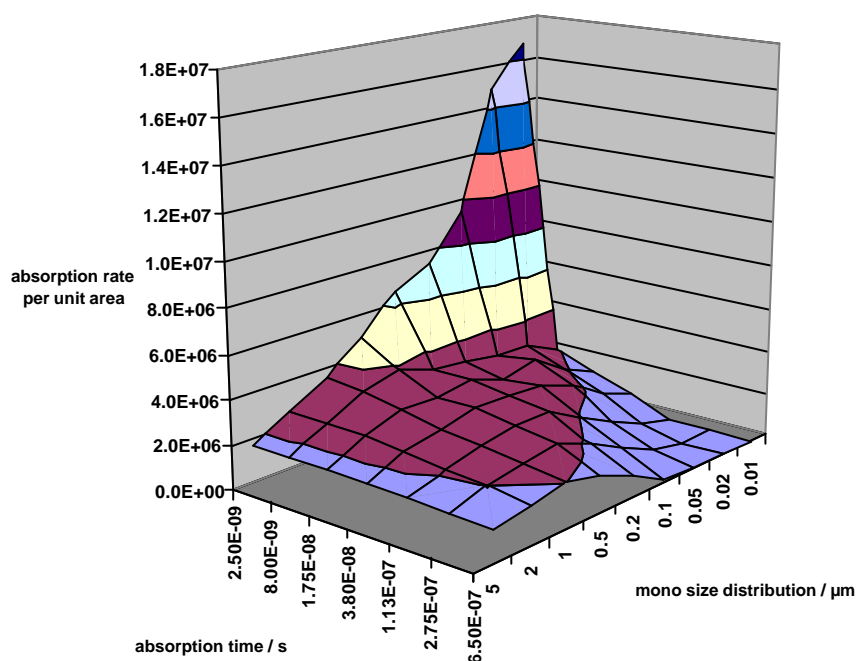


Fig. 11 Rates of absorption (dV/dt) per unit area into a range of monosized Pore-Cor structures observed as a function of time.

There is a peak in the three-dimensional surface showing that the fastest absorption dynamic occurs in the smallest pores at short timescales. This is new information that can only be derived from using an inertial wetting algorithm. It corresponds to observation and contradicts the traditional Lucas-Washburn dynamic. There is a ridge from the finest pores at time zero to a pore size equivalent to $0.1 \mu\text{m}$ after a time of 10 ns which shows the faster rate of absorption. In the case of the smaller pore sizes viscous drag slows the absorption while in the larger pore sizes there is inertial retardation holding back the flow. It can be seen that for these fluid properties there is a preferential size for the maximum flow rate which is the same for both the simulation and the theoretical plot of the direct solution for the Bosanquet equation

for single capillaries shown in Fig 12. This single capillary solution also shows a peak towards zero time at the smallest pore size, and the same ridge of maximum velocity.

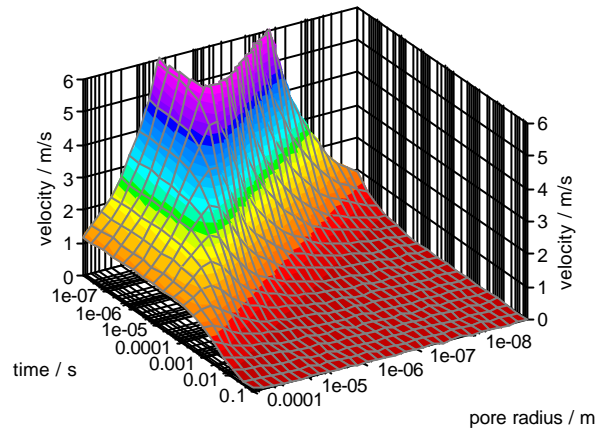


Fig. 12 Bosanquet pore size differentiation favours the pore size which corresponds to the maximum absorption velocity in m/s for water as a function of time.

It can be seen that the effect of inertia is first of all directed toward the exclusion by retardation of all but the finest capillaries from the absorption process close to time $t = 0$. Then the effect of inertia is to favour absorption into those capillaries corresponding to the highest point along the ridge in the three-dimensional surface which progresses away from the origin decaying in magnitude progressively with time. This ridge is shown more clearly in Fig. 13 below.

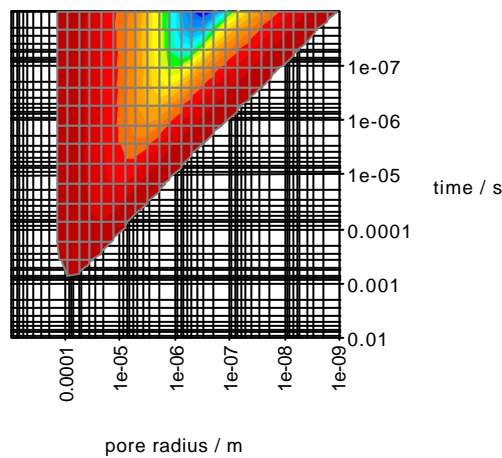


Fig. 13 The “ridge” of maximum absorption velocity for water (z-axis) as a shaded log/log/linear plot; the base z-plane is 1m/s. Fig. 12 shows the same data as a mesh plot.

Having shown, therefore, that the absorption rates of the Pore-Cor *monosized* pore unit cells match the theoretical expectations of the Bosanquet equation for single capillaries it is now possible to use Pore-Cor to predict the behaviour of fluid absorption into these monosize pore structures when the density and viscosity values are changed.

(ii) with changing density at fixed viscosity

The parameters of water were used in the absorption simulation into the 5 μm monosized pore unit cell structure but with a hypothetical progressive reduction in density. The results are shown in Fig. 14.

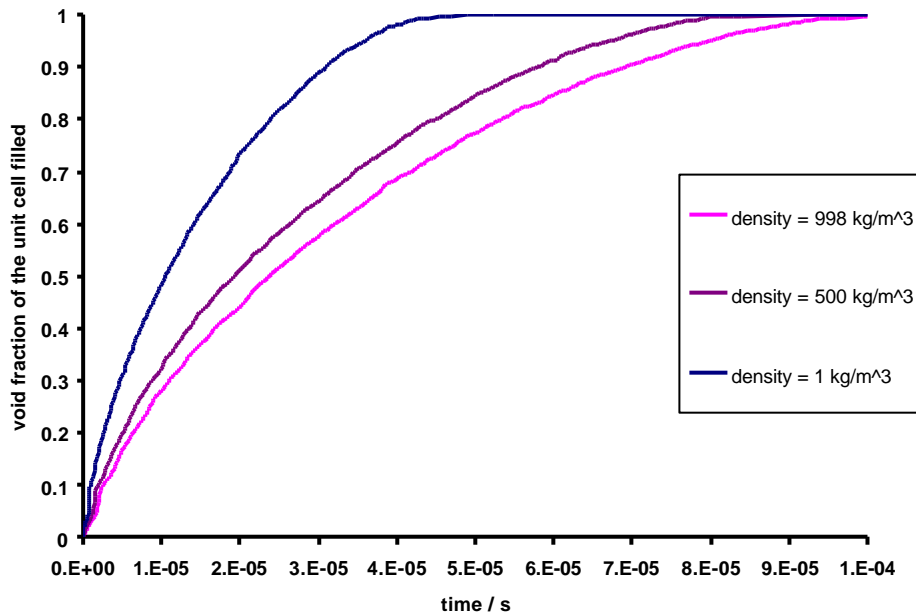


Fig. 14 Absorption into 5 μm monosized Pore-Cor structure as fluid density is reduced.

The absorption rate for a density of 998 kgm^{-3} is seen as the slowest in the plot. This high density simulation shows the behaviour with the inertial delay slowing the absorption. If the density is reduced to 500 kgm^{-3} then the absorption rate increases and a further reduction of density to 1 kgm^{-3} increases the absorption rate toward a maximum which becomes independent of any further decrease in density. This is in effect a Lucas-Washburn limit for an incompressible gas.

The absorption dynamic, i.e. absorption gradient representing the rate of fluid volume absorbed, as a function of pore size is shown in the three-dimensional plots of Fig. 15. These plots illustrate the dependency of the maximum absorption rate on the pore size and density for typical fluid viscosities, e.g. water.

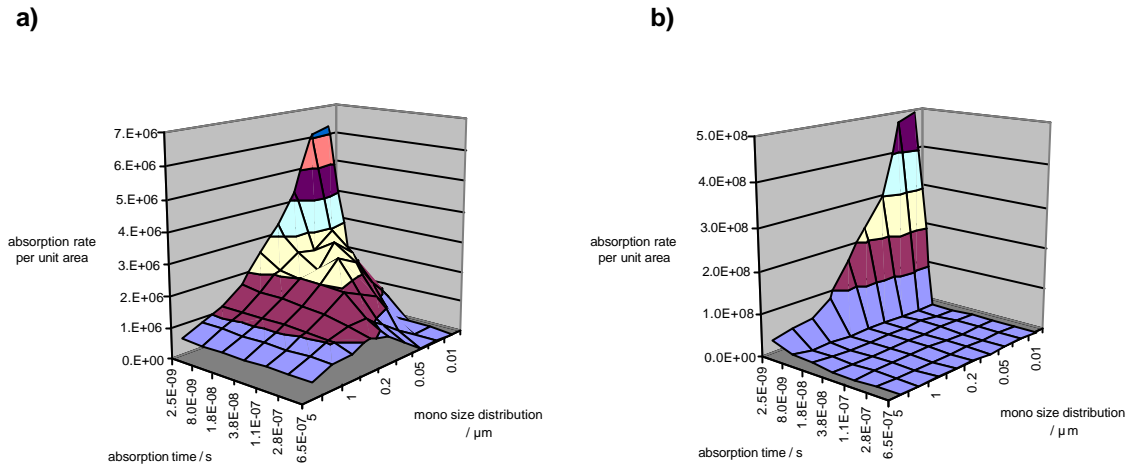


Fig. 15 Rates of absorption (dV/dt) per unit area for different monosized pore structures with a) density = $10\,000\text{ kgm}^{-3}$ and b) density = 1 kgm^{-3} .

As the density decreases so the smaller pore sizes become gradually slower in absorption rate due to the viscous drag as the effect of the inertial linear t regime is lost. However, the larger pore size unit cells have a continuously slower absorption rate due to the inertial retardation. The result is that over a range of practical liquid densities there exists once again the clear ridge of ‘maximum flow’ passing from the origin progressively toward larger pore sizes as time proceeds.

A decrease in density leads to an even higher peak in absorption rate per unit area at the smallest pore size and shortest time, indicating the continued promotion of the linear t regime before viscous drag occurs. At very low density, the difference between the viscous drag and inertial retardation regimes is no longer apparent and so the extended ridge of maximum absorption rate no longer exists.

(iii) at fixed density and changing viscosity

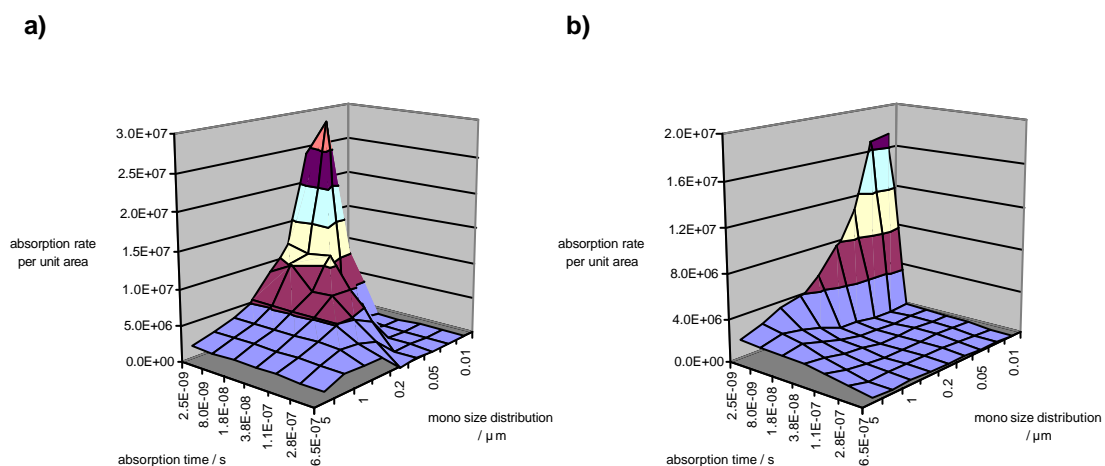


Fig. 16 Rates of absorption (dV/dt) per unit area for different monosized pore structures with a) viscosity = $0.00001\text{ kgm}^{-1}\text{ s}^{-1}$ and b) viscosity = $0.01\text{ kgm}^{-1}\text{ s}^{-1}$.

The surface with the lower viscosity value, Fig. 16, shows a higher peak and a higher ridge area compared to that of water. The viscous drag and inertial retardation slow the flow in the smaller and larger pore size structures respectively but again there is a discernible ridge of 'maximum flow'. The higher viscosity surface shows the same height of peak for the short times in the smallest pore size structure; the peak has moved back to even shorter times and the ridge area has also retreated. The higher viscosity behaviour reflects that of the lower density.

As viscosity increases, the dominance of Lucas-Washburn viscous drag over inertial wetting is evident. The inertial t wetting decays more rapidly as the viscous drag exerts itself. Overall, the rate of absorption slows in general as viscosity increases and only fluids of high density exhibit an absorption dynamic faster than the viscosity would have predicted by classical capillary action.

Monosized pigments in paper coatings

Implications for monosized pigment distributions in paper coatings are more clearly understood when considering these results. The more designers follow the philosophy of monosized pigments and pore structures in an attempt, for example, to optimise light scattering behaviour, the more dangerous becomes the probable discontinuity in absorption between fluids of differing density and viscosity. A selectivity between different fluids can be envisaged which could be used to advantage, but if uncontrolled could lead to the removal of, for example, mineral oil from an ink but not linseed oil. The end effect will be a well-controlled tackification of the ink optimising press runnability but leaving a print on the surface which never sets as the resin remains solved. This can already be suspected in matt coatings (23) and on occasions is now seen to occur in gloss coatings in cases where the philosophy of steep particle size distribution pigments is taken to the extreme.

The effect of these parameters as size distributions change can only be predicted when using a network model in combination with an inertial term as continuum infinite capillaries quickly revert to the viscous drag regime.

Introducing a range of sizes

(i) increasing the range of throat sizes around a common median

In conventional paper coating structures, a range of pore sizes is usually encountered. This breadth of size distribution is an important parameter in balancing the optical properties of a coating layer with its printing properties (24).

It was seen above that water with its relatively high fluid density was insensitive to the fluid retardation maximum as a function of pore size due to a lower viscous drag to inertial wetting ratio. It is important therefore to study effects as pore size distribution broadens in relation to the different fluid properties as it can be expected that different pore sizes differentiate between immiscible fluids, not necessarily because of surface chemistry or wetting effects but because of dynamical

differentiation. This is of particular importance in the offset printing process where fountain solution water and oil-based ink become emulsified.

The size range within a model Pore-Cor structure is here step-wise increased around the central median value of $0.1 \mu\text{m}$ (chosen, as discussed previously, because of its importance as the realistic decay point of the inertial absorption effect for the typical fluid densities and viscosities used in printing). The unit cells have been constructed such that their size, i.e. pore row spacing, Q , has been kept constant, keeping a constant number of throat entries per unit cross-sectional entry area. Again this was effectively achieved by adjusting the porosity as the pore size range was varied, once more following realism. The unit cells are shown in Fig. 17, and the Pore-Cor parameters in Table 5.

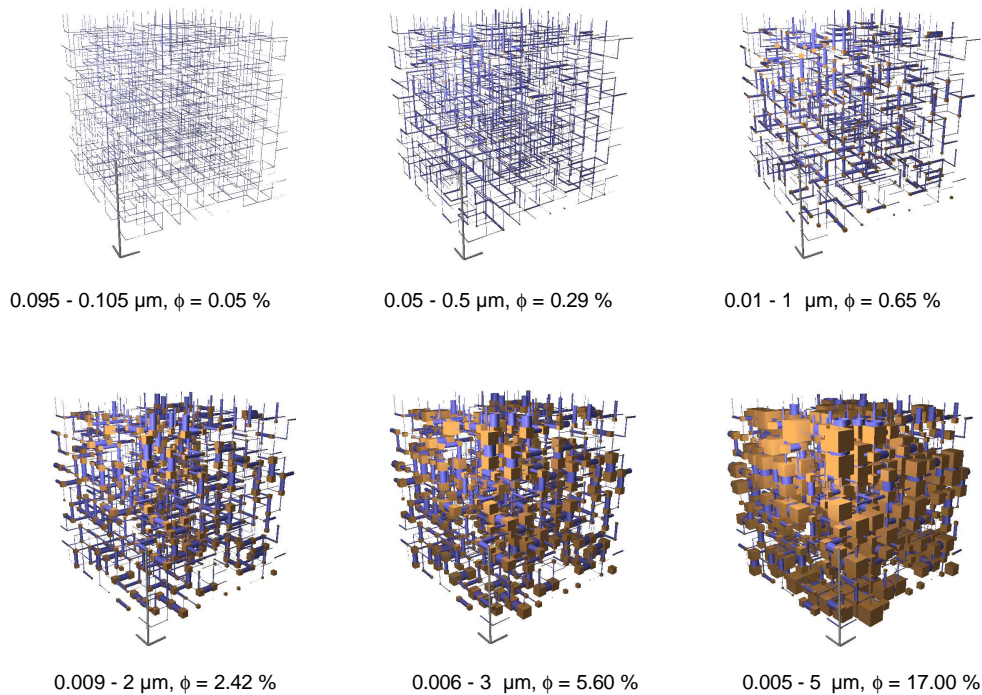


Fig. 17 Generated structures using increasing breadth of pore size distribution centred about $0.1 \mu\text{m}$. Porosity is allowed to increase whilst keeping the pore row spacing constant, i.e. constant number of pore entry features per unit area.

Minimum diameter / μm	Maximum diameter / μm	Throat skew	Connectivity	Porosity, f / %	Pore row spacing, Q / μm
0.095	0.105	1	4	0.05	5.5
0.050	0.500	1	4	0.29	5.5
0.010	1.000	1	4	0.65	5.5
0.009	2.000	1	4	2.42	5.5
0.006	3.000	1	4	5.60	5.5
0.005	5.000	1	4	17.00	5.5

Table 5 Parameters used in the Pore-Cor generations shown in Fig. 17.

To maintain the constant number of entry throats per unit cross-section it is necessary to adopt a unit cell structure in which the throat length associated with the first pores is relatively long so that the viscous retardation in these throats is expected to play a major role (see previous section on long throats).

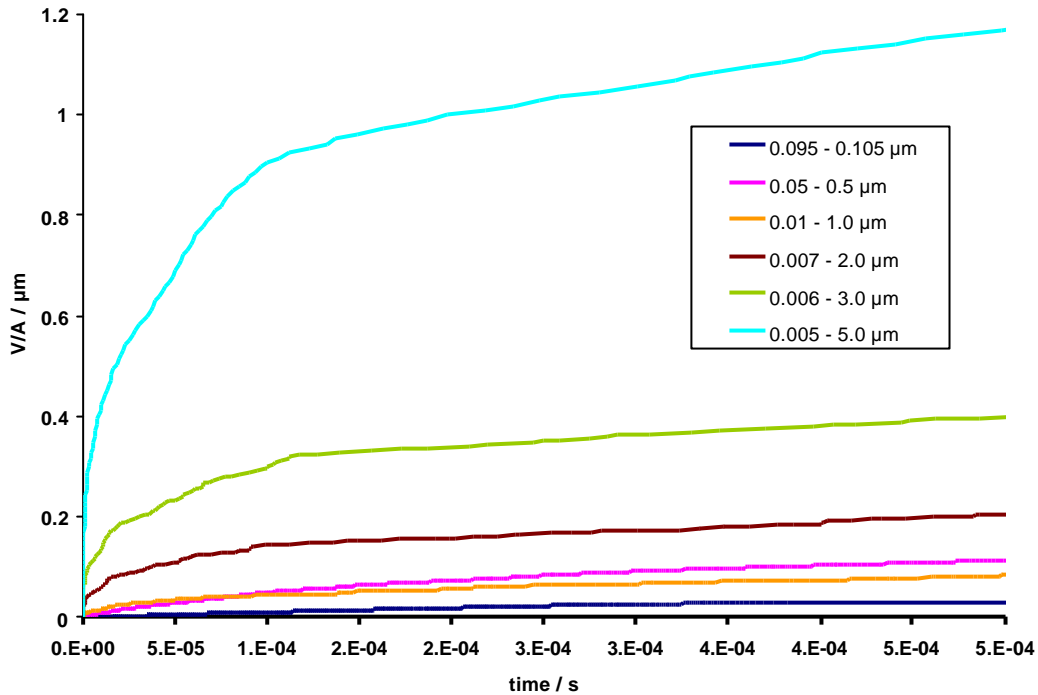


Fig. 18 Effect of breadth of pore size distribution (centred around 0.1 μm) on the absorption of water.

Once again considering the case of water, it is shown in Fig. 18 that, as the throat size distribution is broadened and the porosity increased, the observed volume per unit area absorbed in unit time increases dramatically. This corresponds to reality as reported by ink-setting rate studies (23) and demonstrates that it is not necessary to assume an increase in the number of entry throats as a size distribution broadens in order to explain the increased absorption rate. In the network model the selective absorption occurs first into the finest surface pores. The large pores then follow, providing effective supersource reservoirs for further selective absorption into the next adjacent fine pores. This can be imagined as a fingering of permeation through the distribution of pores.

(ii) extending the range of throat size above and below a median respectively

Two other size ranges are now investigated, one adding in features larger than 0.1 μm (Fig. 19) and the other adding in features smaller than 0.1 μm (Fig. 20), each time keeping the pore row spacing constant so that the number of throat entries per unit area is constant. The Pore-Cor parameters for these structures are shown in Table 6 and Table 7. The limit here is that a self-consistent pore row spacing with each set, i.e. one for increasing throat size and another for decreasing throat size, must be used.

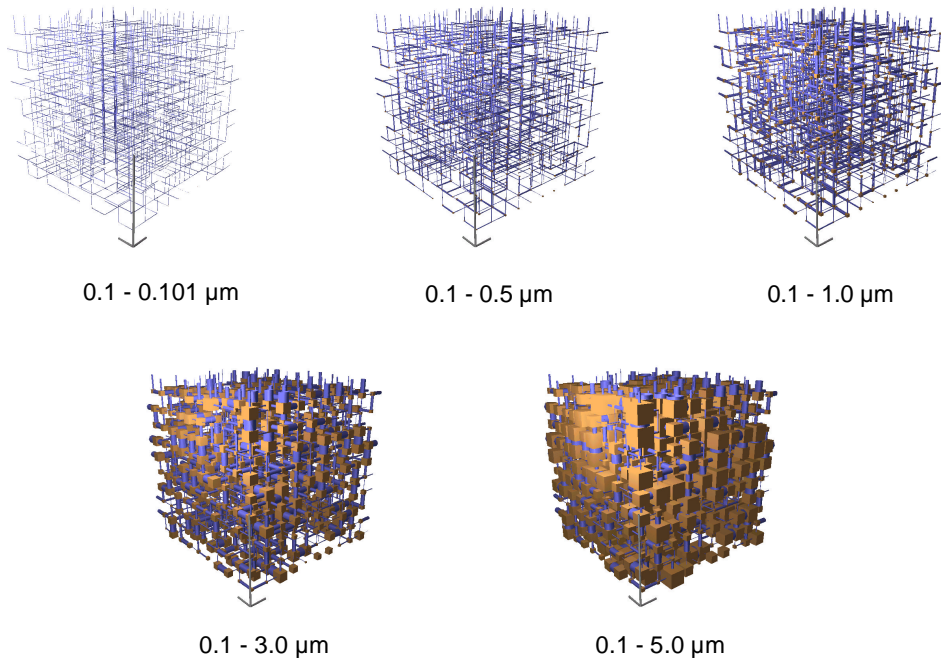


Fig. 19 Unit cell structures with pores and throats extending larger than 0.1 μm , $Q = 5.5 \mu\text{m}$.

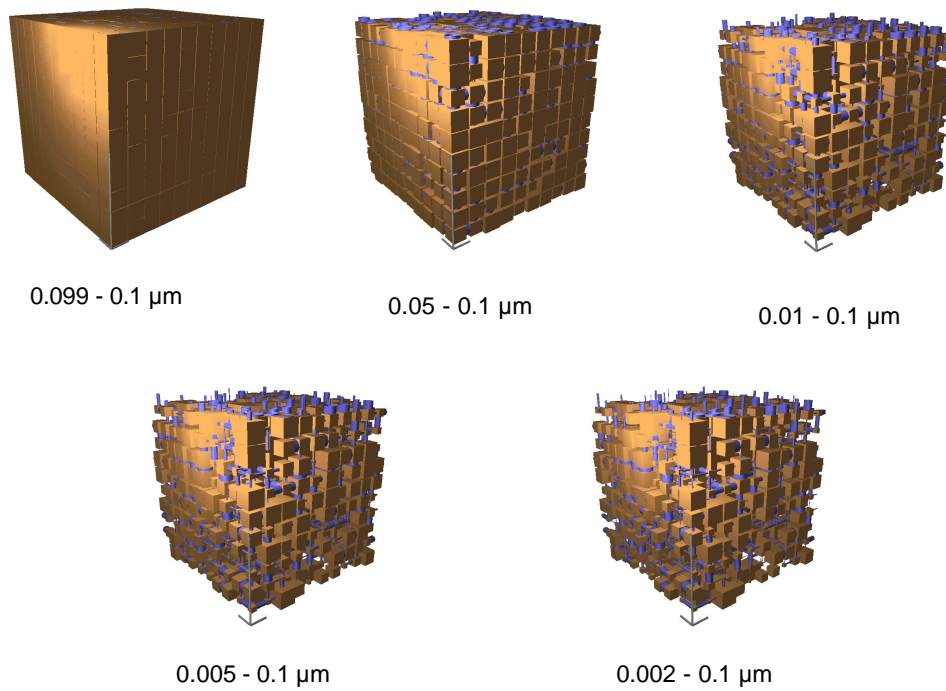


Fig. 20 Unit cell structures with pores and throats extending smaller than 0.1 μm , $Q = 0.1 \mu\text{m}$.

Minimum diameter / μm	Maximum diameter / μm	Throat skew	Connectivity	Porosity, f / %	Pore row spacing, Q / μm
0.1	0.101	1	4	0.05	5.5
0.1	0.500	1	4	0.49	5.5
0.1	1.000	1	4	1.47	5.5
0.1	3.000	1	4	9.10	5.5
0.1	5.000	1	4	30.60	5.5

Table 6 Pore-Cor parameters for the structures extending $\geq 0.1 \mu\text{m}$.

Minimum diameter / μm	Maximum diameter / μm	Throat skew	Connectivity	Porosity, f / %	Pore row spacing, Q / μm
0.099	0.1	1	4	99.0	0.1
0.050	0.1	1	4	77.0	0.1
0.010	0.1	1	4	46.5	0.1
0.005	0.1	1	4	39.4	0.1
0.002	0.1	1	4	32.7	0.1

Table 7 Pore-Cor parameters for structures extending $\leq 0.1 \mu\text{m}$.

It can be seen by comparing Table 6 to Table 7 that, as shown previously, the porosity is greatly increased by decreasing the pore row spacing. It can also be seen, as would be expected, that keeping the pore row spacing constant and increasing the range of sizes results in large porosity changes, i.e. including larger pores increases porosity and vice versa. However, the important structures to compare are those with $0.1 - 5.0 \mu\text{m}$ and $0.002 - 0.1 \mu\text{m}$ size ranges, which, by careful choice of Pore-Cor sizing, have a similar resultant porosity of $\sim 30\%$. It is seen in Fig. 21 that the rate of absorption at the shortest times favours the finest structure whereas at larger times it favours the coarser structure, both at similar porosity. Again this corresponds with accepted reality. In the case of offset ink tackification and setting, the initial tack increase is controlled by the fine pores in a coating structure, and the progression to setting over larger times is a combined function of the remaining retained capillarity and the unfilled porosity resulting in a total void volume of the coating as “seen” by the ink (23).

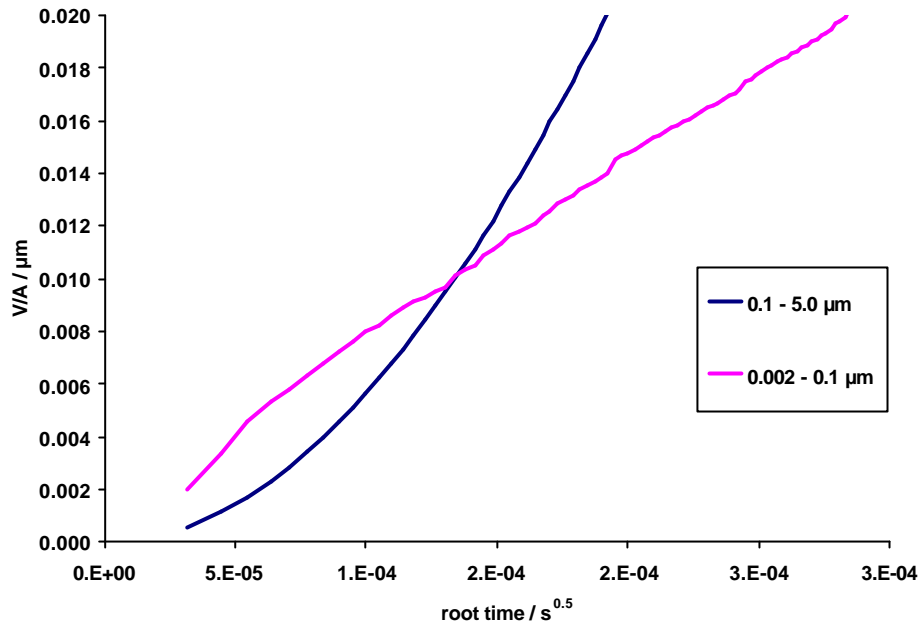


Fig. 21 Short-time absorption for coarse and fine broad pore size distributions at similar porosity.

CONCLUSIONS

This work has shown that the rate of absorption is dependent on many aspects of the geometry of the void structure as well as on the properties of the fluids. It has confirmed that realistic absorption dynamics cannot be modelled using Lucas-Washburn alone. There is a three-dimensional prediction surface showing that the absorption as a function of time depends upon pore size distribution, connectivity and throat length, together with fluid properties such as viscosity and density. This predictor feature, based on the correlations already found between experiment and the modelled results, is shown to be an advance in the initial design of coating structures, independently of expensive machine trials, in that it includes the effects of pore dimension and interstitial structure distributions in particulate systems, and also length of features (eccentricity) in a coating network.

References

1. Gane, P.A.C., Kettle, J.P., Matthews, G.P. and Ridgway, C.J., "Void space structure of compressible polymer spheres and consolidated calcium carbonate paper-coating formulations", *Industrial and Engineering Chemistry Research*, 35(5):1753-1764 (1995).
2. Gane, P.A.C., Schoelkopf, J., Spielmann, D.C., Matthews, G.P. and Ridgway, C.J., "Observing fluid transport into porous coating structures: some novel findings", *Tappi Journal*, 85(5):1-3 (2000).
3. Schoelkopf, J., Ridgway, C.J., Gane, P.A.C., Matthews, G.P. and Spielmann, D.C., "Measurement and network modelling of liquid permeation into compacted mineral blocks", *Journal of Colloid and Interface Science*, 227(1):119-131 (2000).

4. Ridgway, C.J., Schoelkopf, J., Matthews, G.P., Gane, P.A.C. and James, P., *The effects of void geometry and contact angle on the absorption of liquids into porous calcium carbonate structures*", submitted to Journal of Colloid and Interface Science, (2000).
5. Schoelkopf, J., Gane, P.A.C., Ridgway, C.J. and Matthews, G.P., *"Influence of inertia on liquid absorption into paper coating structures"*, Nordic Pulp and Paper Research Journal, 15(5):422-430 (2000).
6. Gane, P.A.C., *"New flexibility for print-surface design from 100% natural ground calcium carbonate"*, Tappi Coating and Papermakers Conference, New Orleans, Tappi Press, Atlanta (1998).
7. Rousu, S.M., Gane, P.A.C., Spielmann, D.C. and Eklund, D.E., *"Separation of offset ink components during absorption into pigment coating structures"*, Nordic Pulp and Paper Research Journal, 15(5):527-553 (2000).
8. Rousu, S.M., Gane, P.A.C., Spielmann, D.C. and Eklund, D.E., *"Differential absorption of offset ink components on coated paper"*, International Printing and Graphic Arts Conference, Savannah, Georgia, Tappi Press, Atlanta (2000).
9. Burri, P., Spielmann, D.C., Naydowski, C. and Swanson, E.T., *"From theory to practice - Use of classical theory to design a pigment with improved optical properties"*, 1996 Coating Conference Proceedings, Tappi Press, Atlanta, 203-213 (1996).
10. Donigian, D.W., Ishley, J.N. and Wise, K.J., *"Coating pore structure and offset printed gloss"*, Tappi Coating Conference Proceedings, 39-48 (1996).
11. Preston, J., Daun, M. and Nutbeam, C., *"Attaining print performance through pigment engineering"*, 19th PTS Coating Symposium, Munich, (1999).
12. Gane, P.A.C., Buri, M. and Blum, R., *"Pigment co-structuring: New opportunities for higher brightness coverage and print surface design"*, International Symposium on Paper Coating Coverage, Helsinki, AEL METSKO, Finland, (1999).
13. Bosanquet, C.M., *"On the flow of liquids into capillary tubes"*, Phil. Mag., S6 45(267):525-531 (1923).
14. Matthews, G.P., Ridgway, C.J. and Small, J.S., *"Modelling of simulated clay precipitation within reservoir sandstones "*, Marine and Petroleum Geology, 13(5):581-589 (1996).
15. Ridgway, C.J., Ridgway, K. and Matthews, G.P., *"Modelling of the void space of tablets compacted over a range of pressures"*, Journal of Pharmacy and Pharmacology, 49:377-383 (1997).

16. Peat, D.M.W., Matthews, G.P., Worsfold, P.J. and Jarvis, S.C., "*Simulation of water retention and hydraulic conductivity in soil using a three-dimensional network*", European Journal of Soil Science, 51(1):1-15 (2000).
17. Matthews, G.P., Ridgway, C. J. and Spearing, M.C., "*Void space modeling of mercury intrusion hysteresis in sandstone, paper coating, and other porous media*", Journal of Colloid and Interface Science, 171(1):8-27 (1995).
18. Lucas, R., "*Ueber das Zeitgesetz des kapillaren Aufstiegs von Fluessigkeiten*", Kolloid Z., 23:15 (1918).
19. Washburn, E.W., "*The dynamics of capillary flow*", Physical Review, 17:273-283 (1921).
20. Rideal, E.K., "*On the flow of liquids under capillary pressure*", Phil. Mag., 1152-1159 (1922).
21. Quéré, D., "*Inertial capillarity*", Europhysics Letters, 39(5):533-538 (1997).
22. Knackstedt, M.A., Senden, T.J. and Lyne, M.B., "*The dependence of printing on liquid penetration into paper: the role of pore morphology and surface chemistry*", Paper and Coating Chemistry Symposium 2000, Stockholm, Sweden, (2000).
23. Gane, P.A.C., Seyler, E.N. and Swan, A., "*Some novel aspects of ink/paper interactions in offset printing*", International Printing and Graphic Arts Conference, Halifax, Nova Scotia, CPPA, Montreal, Canada, 209-228 (1994).
24. Gane, P.A.C., "*Mineral pigments for paper: Structure, function and development potential*", Wochenblatt für Papierfabrikation, to be published (2000).